Journal of Photochemistry & Photobiology, B: Biology 202 (2020) 111673

Contents lists available at ScienceDirect

Journal of Photochemistry & Photobiology, B: Biology

journal homepage: www.elsevier.com/locate/jphotobiol

Structure of photo-damaged white and naturally pigmented human hair

M. Richena[a,*], C.A. Rezende[b]

[a] AgResearch, Lincoln Research Centre, AgResearch Ltd, Private Bag 4749, Christchurch 8140, New Zealand
[b] Institute of Chemistry, University of Campinas – UNICAMP, Campinas, Brazil

ARTICLE INFO

Keywords:
Human hair
Keratin
Photo-damage
Lipids

ABSTRACT

The effect of photo-degradation processes on the morphology and ultrastructure of pigmented and non-pigmented hair was evaluated in this work by small angle X-ray scattering (SAXS) and transmission electron microscopy (TEM). Samples consisted of three types of grey hair (separated out into subsamples of totally white and totally black strands) and one type of dark-brown hair exposed to solar irradiation for 75 h or to a mercury lamp for 600 h.

SAXS patterns showed that irradiation mainly damaged the amorphous regions of hair, and in some types of hair, an ordered structure appeared, with spaces of *ca.* 4.5 nm. This structure occurred independently of the presence of pigments and its scattering intensity increased after irradiation. Layers of lipids present in the cuticle may be responsible for this scattering around 4.5 nm, as indicated by TEM images. TEM also showed morphological changes in the outermost cuticle layers, such as the degradation of endocuticle and the detachment of the cell membrane complex. Therefore, the results presented herewith showed that irradiation caused different damages to the hair amorphous fractions, especially in the cuticle layers, which are the most exposed areas of the hair strands.

1. Introduction

Solar radiation is responsible for changes in the ultrastructure of human hair [1–3], since proteins, lipids and melanin pigments interact with light, starting a cascade of damage to hair morphology [4–6]. In order to prevent undesirable effects, such as colour changes, split ends, loss of shine and loss of mechanical strength, it is important to understand how solar radiation interacts with the complex morphological structure of human hair.

Hair consists of organised and amorphous structures and its main components are cuticle, cortex and the cell membrane complex (Fig. 1). Each cuticle cell is formed by amorphous material and is divided into epicuticle, a-layer, exocuticle and endocuticle layers (Fig. 1c) that have distinct hydrophilicity and chemical composition [7–9]. The outermost layer of the cuticle cell is epicuticle, which is hydrophobic and cystine-rich (≈ 12% *w*/w). Then, the second and third layers are a-layer and the exocuticle, which are more reticulated and hydrophobic, containing higher amounts of cystine (≈ 30% and ≈ 15% *w*/w, respectively). Finally, the most internal layer is the endocuticle, which is hydrophilic and composed of non-keratinous material (≈ 3% w/w cysteine) [10].

Cell membrane complex (CMC) has the adhesive role of binding the cuticle-cuticle, cuticle-cortex and cortex-cortex cells together [11] (Fig. 1c and d). The general structure of the CMC has a central hydrophilic δ-layer (15–18 nm in thickness), which is composed of proteins and polysaccharides, and is covered on both sides by hydrophobic lipid layers (≈ 5 nm in thickness each), called the inner β-layer (located between endocuticle and δ-layer) and the outer β-layer (adjacent to the epicuticle) [7]. Cuticle-cuticle CMC contains monolayer lipids that are attached by covalent bonds to proteins in the cuticle and by Van der Waals attractive forces to the δ-layer [11]. The inner β-layer contains mainly palmitic, stearic and oleic fatty acids, while the outer β-layer has 18-methyl eicosanoic acid (18-MEA), as the main component [12–14]. The outer β-layer is also the most external part of the strand and the one most exposed to environmental action, thus having an important role in hair protection.

The cortex fills the core of the strand and consists of organised (fibrils) and amorphous (matrix) keratin structures (Fig. 1d). Fibrils are embedded in the high sulphur protein matrix (or intermicrofibrillar matrix), forming an ultrastructure called a macrofibril. The organisation of the macrofibril extends down in several scales: macrofibrils (≈ 200 nm in diameter) are composed of microfibrils (≈ 7 nm in diameter), which are formed by protofibrils (≈ 4.5 nm in diameter) [7,15], which in turn, contain protofilaments (≈ 2 nm in diameter), formed by protein α-helices [16–18]. The cortex also contains melanin granules (Fig. 1d) which are responsible for the hair colour and are assumed to have a photo-protective role [10], although they are present

* Corresponding author.
E-mail address: marina.richena@agresearch.co.nz (M. Richena).

https://doi.org/10.1016/j.jphotobiol.2019.111673
Received 15 February 2019; Received in revised form 20 August 2019; Accepted 24 October 2019
Available online 31 October 2019
1011-1344/

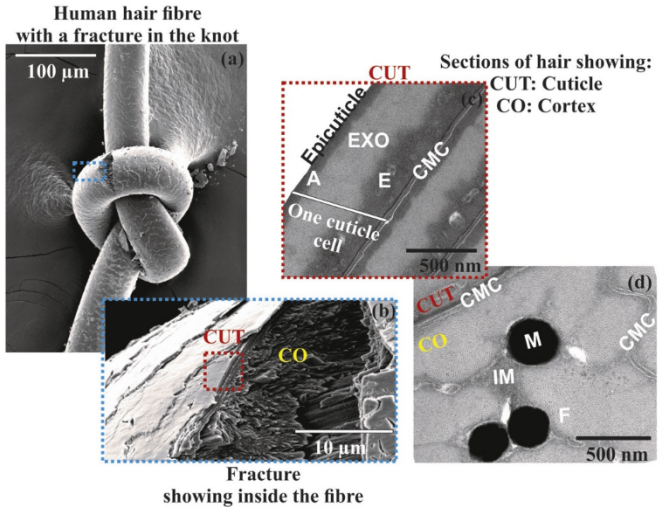

Fig. 1. Images of human hair fibre. (a) Scanning electron micrograph of a hair with a knot in the central region, where the blue rectangle highlights part of a fracture in the knot and (b) fracture showing the cuticle (CUT indicated by brown rectangle) and the cortex (CO); (c) transmission electron micrograph of a cross-section of a cuticle showing one cuticle cell that contains a-layer (A), exocuticle (EXO), endocuticle (E) and cell membrane complex (CMC); (d) cortex with fibrils (F), intermicrofibrillar matrix (IM), CMC and melanin granules (M). (For interpretation of the references to colour in this figure legend, the reader is referred to the web version of this article.)

in the interior of the cortex, far from the irradiated hair surface.

Severe chemical and physical damages caused by irradiation to the fibre structure have already been described [[19–28]]. Robbins and Bahl [19] showed that ultraviolet (UV) radiation is primarily responsible for weathering degradation of hair (depth within 20 to 30 Å). They concluded that weathering of human hair involves the degradation of cystine residues and that UV radiation caused more damage to the surface than to the core of the strand. In previous work, we analysed the effect of UV radiation on the hair surface [2,3] using atomic force microscopy, field emission scanning electron microscopy and transmission electron microscopy (TEM). Atomic force microscopy [2] showed that the morphology of the cuticle is significantly modified after irradiation, resulting, for instance, in detachment of the cuticle scales. This result may be caused by degradation of the internal cuticle layers (CMC and epicuticle) since they are responsible for the adhesive contact between overlapping cuticles. Field emission scanning electron microscopy combined to TEM revealed that photo-degradation leads to the formation of cavities in the endocuticle (with diameters of 50–700 nm) and to the detachment of the outer β-layer, present in the CMC [3]. These analyses showed that irradiation significantly alters the morphology of the cuticle, within which the most degraded structures are the epicuticle, the endocuticle and the CMC.

The present paper brings new data showing the location of photo-irradiation damage in the hair structure. The interaction of irradiation and melanin was also evaluated, by analysing both pigmented and non-pigmented hair. This work thus contributes to the body of knowledge on changes in the organised and amorphous phases of the hair strands after photo-degradation.

2. Material and Methods

2.1. Samples

Blended grey and dark-brown hair were purchased from De Meo Brothers Inc. (New York, USA). Grey hair was also collected from two volunteers with no history of chemical treatments (called grey hair from single-donor in the text). Grey hair is a mixture of totally white and totally black strands, which were separated by hand. Prior to the experiments, hair samples were washed as previously described [28].

2.2. Free Lipids Extraction

Free lipids were extracted from dark-brown hair with ethyl ether in a Soxhlet extractor for 72 h. After complete evaporation of the solvent containing the free lipids inside a desiccator, these were re-suspended in a 12 mM tris-HCl buffer (pH = 7.2) and sonicated.

2.3. Radiation Sources

Two types of radiation sources were used: 1) direct sunlight and 2) mercury vapour lamp (OSRAM HQL 125 W, São Paulo, Brazil). The overall procedure for irradiation and measurements of light intensity are described elsewhere [28].

2.3.1. Exposure to Solar Radiation

Hair samples were exposed to solar full spectrum for 5 h, followed by a period in the dark (> 19 h) on sunny days in Campinas, Brazil (22°53' S; 47°04' W). The total exposition time was 75 h. The detailed experimental procedure is described in reference [28]. The average values of local temperature and relative humidity during the experiments were 33 ± 4 °C and 44 ± 13%, respectively. The values of radiation intensity obtained for sunlight at 12 pm were: 2.3 ± 0.3 $W\,m^{-2}$ (UVB), 31 ± 8 $W\,m^{-2}$ (UVA), 148 ± 14 $W\,m^{-2}$ (VIS) and 557 ± 19 $W\,m^{-2}$ (IR).

2.3.2. Exposure to Artificial Radiation

Hair samples were exposed to the mercury vapour lamp full-spectrum for 10 h, followed by > 14 h in the dark, totalizing 600 h of irradiation. Details about the irradiation procedure can be found in [23]. The averages of temperature and relative humidity were 29 ± 1 °C and 44 ± 5%, respectively. The values of radiation intensity obtained for the lamp were: 0.5 ± 0.1 $W\,m^{-2}$ (UVB), 16 ± 5 $W\,m^{-2}$ (UVA), 27 ± 1 $W\,m^{-2}$ (VIS) and 31 ± 3 $W\,m^{-2}$ (IR). Comparing the daily doses of UV radiation from the lamp and the sun [3], 5 h of sun exposure (at 12 h, summer period) are equivalent to ≈ 10 h of irradiation by the UV mercury lamp (≈ 59×10^4 $J\,m^{-2}$).

2.4. Small Angle X-Ray Scattering (SAXS)

SAXS experiments were performed at the Brazilian Synchrotron Light Laboratory (LNLS), located in Campinas-SP, Brazil. The X-ray energy was 8.00 KeV and the wavelength was 1.55 Å. The distances between the sample and the MAR-165 detector were based on the second-order diffraction ring in the scattering pattern from silver behenate (d-spacing = 58.380 Å [29]), which were 1.5 m (30 s of exposure time) and 0.5 m (120 s of exposure time). Image plates have 316 × 316 pixels and 79 × 79 µm. The beam size was 3 mm in the horizontal direction and 2 mm in the vertical one. Two types of sample preparation were carried out: 1) about 100 strands were lined up in the sample holder; and 2) one drop of free lipids solution (extraction procedure in section 2.2) was deposited on a thin mica support and dried at room temperature. For each SAXS pattern, air contribution was subtracted by measuring an empty sample holder. The SAXS pattern was processed using the Fit2D software.

2.5. Transmission Electron Microscopy (TEM)

TEM images were obtained in a FEI Morgagni microscope operating at 80 kV, using a sample preparation designed to minimise hair intrinsic morphological variability [3]. In brief, three hair strands were selected per treatment and each strand was cut in two halves. While one half was exposed to irradiation, the other one served as the control. Both the untreated and treated parts of the strand were fixed, dehydrated,

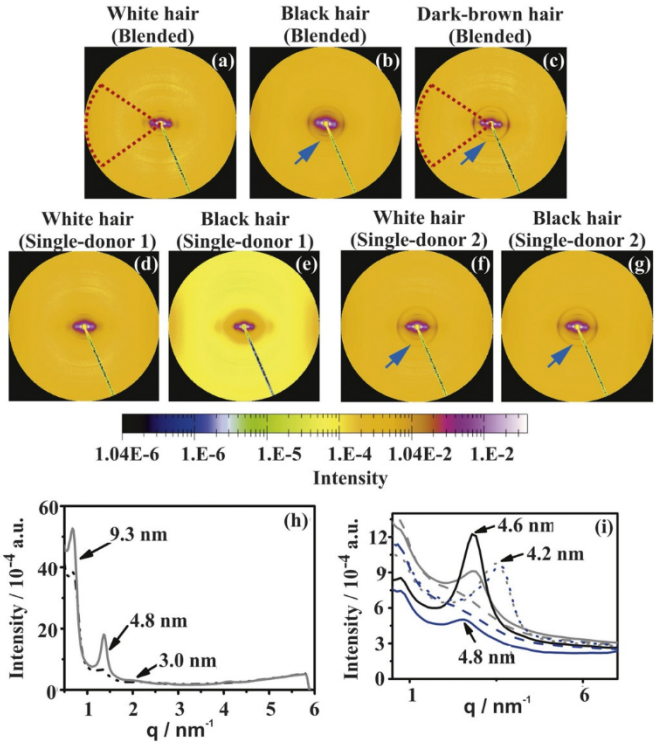

Fig. 2. SAXS patterns of about 100 strands were analysed in each sample. (a) blended white strands from grey hair; (b) blended black strands from grey hair; (c) blended dark-brown hair; (d) single-donor 1 white strands from grey hair; (e) single-donor 1 black strands from grey hair; (f) single-donor 2 white strands from grey hair; and (f) single-donor 2 black strands from grey hair. Blue arrows indicate the presence of rings scattering in (b), (c), (f) and (g). (h) One-dimensional equatorial intensity profiles extracted from SAXS patterns of blended white (– – -) and dark-brown (—) (red circle sectors in (a) and (c)). Three peaks (at 9.3 nm, 4.8 nm and 3.0 nm) are visible perpendicular to the fibre axis (equator), but the peak at 4.8 nm is superimposed to a ring in some samples (blue arrow in (b), (c), (f) and (g)). (i) One-dimensional azimuthal intensity profiles extracted from SAXS patterns (a-g), (—) blended white; (—) blended black; (—) blended dark-brown; (– – -) single-donor 1 white; (– – -) single-donor 1 black; (····) single-donor 2 white and (····) single-donor 2 black. Sample-detector distance was 0.5 m (q range: 0–6 nm^{-1}). (For interpretation of the references to colour in this figure legend, the reader is referred to the web version of this article.)

embedded in resin, sectioned and then stained [3].

3. Results and Discussion

3.1. Structure of Human Hair before Irradiation

SAXS patterns were obtained in this work to study the organised structure of human hair (Fig. 2) prior to irradiation and with different pigmentation levels. Three types of hair samples were used for this purpose: 1) white strands from grey hair; 2) black strands from grey hair; and 3) dark-brown hair.

Fig. 2(a–g) shows the SAXS patterns obtained from blended grey (Fig. 2a and b), blended dark-brown (Fig. 2c), single-donor 1 grey (Fig. 2d and e) and single-donor 2 grey hairs (Fig. 2f and g). Grey hair was separated into totally white (a, d and f) and totally black (Fig. 2b, e and g) strands. Fig. 2(h) shows equatorial intensity profiles extracted from SAXS patterns of blended white and dark-brown hair strands, indicated by the red circle sectors in (Fig. 2a and c). Fig. 2(i) shows azimuthal intensity profiles extracted from SAXS patterns in all the hair types.

The equatorial pattern for human hair diffraction is the superposition of the diffraction patterns of all finite and infinite lattices in the perpendicular direction of the fibre axis. Organised structures lead to organised scattering patterns, transformed into peaks, which indicate the separation distance of the structures (related to their size). On the other hand, amorphous materials result in random scattering, without peaks. Three peaks are visible in the equatorial pattern in all types of hair: at 9.3 nm; at 4.8 nm and at 3.0 nm, as shown in Fig. 2(h) for blended white and dark-brown hair. The peak at 9.3 nm is related to the separation distance of microfibrils, while the 3.0 nm peak is assigned to the separation between protofilaments. The peak at 4.8 nm is attributed to the separation distance of protofibrils, which in some types of hair is superimposed to a ring signal (as indicated by blue arrows in Fig. 2b, c, f and g). The values of these peaks vary between the hair samples, due to differences in the content of the matrix surrounding the microfibrils. Matrix is amorphous and causes a diffuse scattering, which can be observed below the peaks in Fig. 2(h).

The main difference between the SAXS patterns obtained is a ring scattering around 4.5 nm, due to organised structures separated by about this distance. This ring is present in some types of hair (blue arrows in Fig. 2b, c, f and g) and absent in others (Fig. 2a, d and e). Within the group of samples analysed here, the ring can be observed in blended dark-brown hair, in black strands from blended and single-donor 2 and in white strands from single-donor 2. White strands from blended hair and white or black strands from single-donor 1 do not show the scattering ring. Fig. 2(i) shows azimuthal profiles from the SAXS patterns (Fig. 2a–g) in the q range of the ring scattering. The position of the ring varied from 4.8 nm to 4.5 nm and 4.2 nm for blended dark-brown, blended black and white and black strands from single-donor 2, respectively. Therefore, although this ring signal is mostly present in pigmented hair (black and dark-brown), we do not believe that it could be attribute to the hair pigmentation, because an intense ring at 4.2 nm also appeared in one of the white hair samples (blue arrow in Fig. 2f). TEM analysis showed that all the white hair samples used in this study have a small remaining amount of melanin pigments in their cortex. All the samples showing similar quantities of this remaining melanin. Furthermore, statistical analysis would be required to answer this question properly. A morphological description of blended white strands is presented in reference [28], showing the remaining melanin pigments in white hair structure. Though the ring scattering effect has been known since 1963 [30], its origin is still uncertain. Wilk et al. [31] considered that the set of diffuse arcs, indexed onto a spacing of 4.42 nm, is consistent with that expected from a disordered array of high sulphur protein conglomerates (contained within the matrix) or possibly from lipids. Then, two other papers from different authors [32,33] observed that hair from breast-cancer patients has a different intermolecular structure as compared to the hair from healthy individuals. This difference was reported as the presence of a ring corresponding to a spacing of 4.44 nm on the pattern obtained from breast cancer patients. They concluded that this pattern arises from randomly orientated lipid bilayers, either in the plasma membrane or in membranous inclusions in hair cells and proposed that single hair SAXS results might lead to a screening method for breast cancer. Furthermore, this ring was also observed in patterns from individuals “not yet diagnosed with breast cancer but suspected of being at risk”. Brik et al. [34] tried to repeat the study using a different hair sample, but were unable to replicate the observations of the first work. In another study [35] using X-ray microdiffraction, this ring was attributed to lipids, mainly located in the outer layers of the fibre.

3.1.1. Investigation of the Ring around 4.5 nm

The ring around 4.5 nm is generally attributed in the literature to lipids present in hair structure [36]. Lipids represent around 2% by weight of human hair and can be found in the form of: 1) free lipids, which are bounded to keratin by salt linkages or polar bonding; or 2) covalently-bound lipids, which are the ones that are attached to keratin of the cell membranes by covalent bonds on one end and by van der Waals attractive forces on the other end [11]. Free lipids were extracted

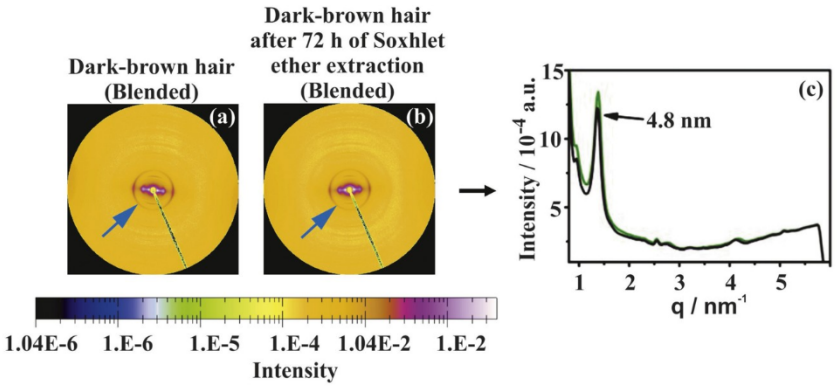

Fig. 3. SAXS patterns of about 100 strands of blended dark-brown hair were analysed: (a) before and (b) after 72 h of Soxhlet ether extraction. (c) One-dimensional azimuthal intensity profiles extracted from SAXS patterns of dark-brown hair before (—) and after (—) ether extraction. Ring intensity at 4.8 nm is not reduced after free lipids extraction in dark-brown hair. Sample-detector distance was 0.5 m (q range: 0–6 nm − 1). (For interpretation of the references to colour in this figure legend, the reader is referred to the web version of this article.)

from dark-brown hair with hot ether extraction (Soxhlet) for 72 h. Dark-brown hair was chosen due to its strong ring scattering around 4.5 nm (Fig. 2(c)). Fig. 3 shows SAXS patterns of blended dark-brown hair before (Fig. 3a) and after (Fig. 3b) 72 h of Soxhlet ether extraction. After the extraction of free lipids, the ring is still present in the SAXS pattern, as indicated by the blue arrows in Fig. 3 (a) and (b). The intensity of the ring (12.5 × 10 − 4 a.u.) is not reduced after the solvent extraction, as shown in the azimuthal intensity profiles in Fig. 3(c). This result shows that the ring scattering around 4.5 nm cannot be attributable to free lipids contained within the hair structure.

A SAXS pattern obtained in free lipids extracted from dark-brown hair and re-suspended in 12 mM tris-HCl buffer (pH = 7.2) is shown in Fig. 4(a), where the presence of a ring with low intensity (blue arrow in Fig. 4(a)) can be noticed. The ring scattering in this case corresponds to a molecular spacing of 7.7 nm (Fig. 4(b)), thus reinforcing that the ring around 4.5 nm should not be correlated to the organisation of the free lipids indeed. Corroborating these results, Cordech et al. [37] studied free lipids extracted from untreated hair using SAXS and observed that they are ordered with a diffraction distance between 7 and 10 nm, which depends on the molecular size of the lipids.

Furthermore, the ring scattering at 7.7 nm is not present in the SAXS patterns of hair shown in Figs. 2 and 3, thus indicating that these free lipids could be ordered after their extraction from hair.

In conclusion, SAXS patterns showed that there is an ordered structure causing a ring scattering around 4.5 nm in some types of hair before irradiation. The origin of this ring scattering could not be determined, but the results presented here showed that it could not be related to hair pigmentation or to free lipids. They could be related to covalently bonded lipids on the other hand.

3.2. Characterization of Hair after Irradiation

3.2.1. Small Angle X-Ray Scattering (SAXS)

Fig. 5 shows the SAXS patterns obtained in hair before (Fig. 5a–c) and after 600 h of irradiation with a mercury vapour lamp (Fig. 5d–f).

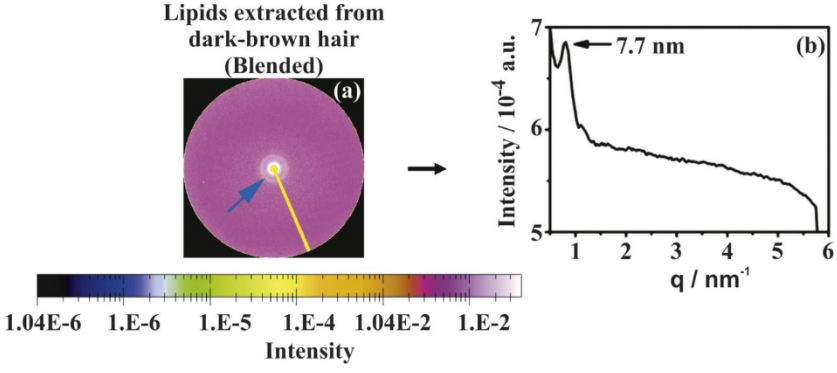

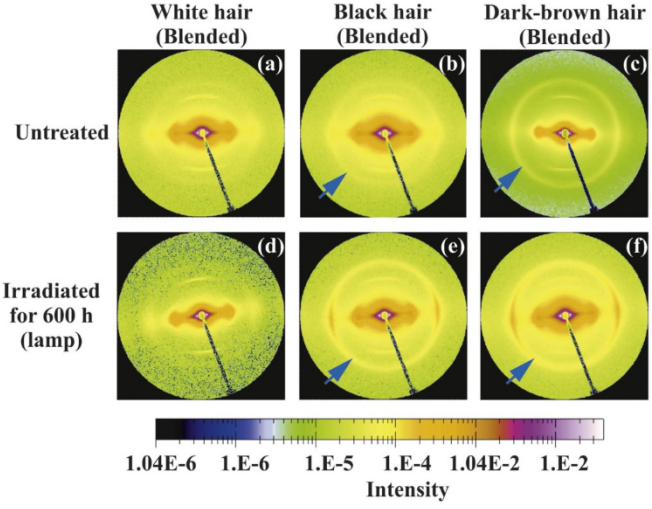

Fig. 5. SAXS patterns of human hair (a-c) before and (d-f) after 600 h irradiation with a mercury lamp: (a) and (d) white and (b) and (e) black strands from blended grey hair; (c) and (f) blended dark-brown strands. Blue arrows indicate the ring scattering around 4.5 nm. Sample-detector distance was 1.5 m (q range: 0–3 nm − 1). (For interpretation of the references to colour in this figure legend, the reader is referred to the web version of this article.)

The corresponding equatorial intensity profiles are shown in Fig. 6(a–c) and the azimuthal intensity profiles in Fig. 6(d–f) for untreated and irradiated hair. Two peaks are visible in the equatorial region in SAXS patterns in Fig. 6(a–c): at 9.3 nm and at 4.8 nm, which are attributed to microfibrils and protofibrils, respectively. After irradiation, these two peaks continue in the same position (arrows in Fig. 6(a–c)). Furthermore, there is diffuse scattering caused by amorphous regions within the hair structure, as can be observed below the peaks in Fig. 6(a–c). After 600 h of irradiation, there is a decrease in the diffuse scattering, as evidenced by the decrease in the intensity of the curves around 9 nm.

Fig. 4. (a) SAXS pattern of free lipids extracted from dark-brown hair and re-suspended in 12 mM tris-HCl buffer (pH = 7.2); (b) One-dimensional azimuthal intensity profiles extracted from SAXS pattern. Blue arrow in (a) indicates the ring scattering at 7.7 nm. Sample-detector distance was 0.5 m (q range: 0–6 nm − 1). (For interpretation of the references to colour in this figure legend, the reader is referred to the web version of this article.)

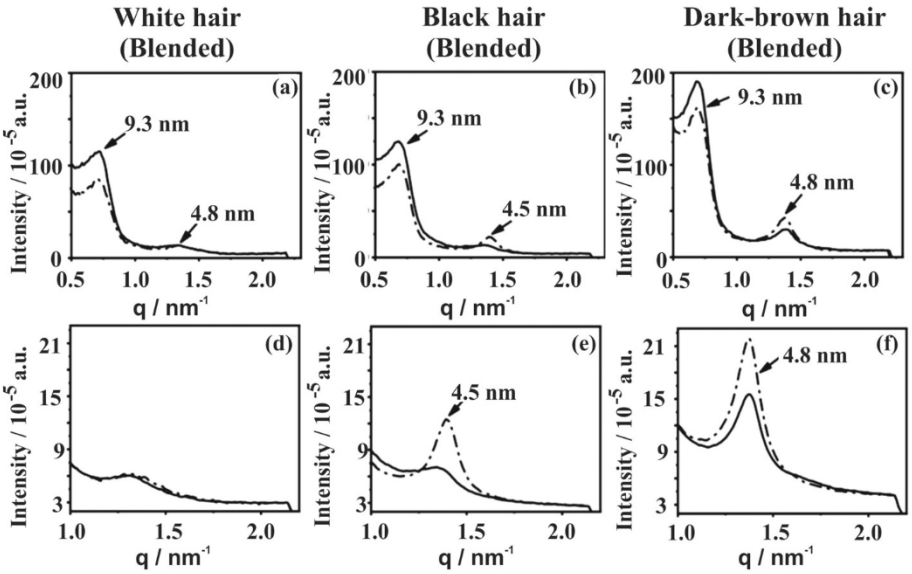

Fig. 6. One-dimensional intensity profiles extracted from SAXS patterns of human hair in Fig. 5: (a-c) equatorial profiles and (d-f) azimuthal profiles. Hair types analysed are (a) and (d) white strands from blended grey hair; (b) and (e) black strands from blended grey hair; (c) and (f) blended dark-brown hair, (—) untreated or (– – -) irradiated for 600 h with a mercury lamp. Sample-detector distance was 1.5 m (q range: 0–3 nm − 1). (For interpretation of the references to colour in this figure legend, the reader is referred to the web version of this article.)

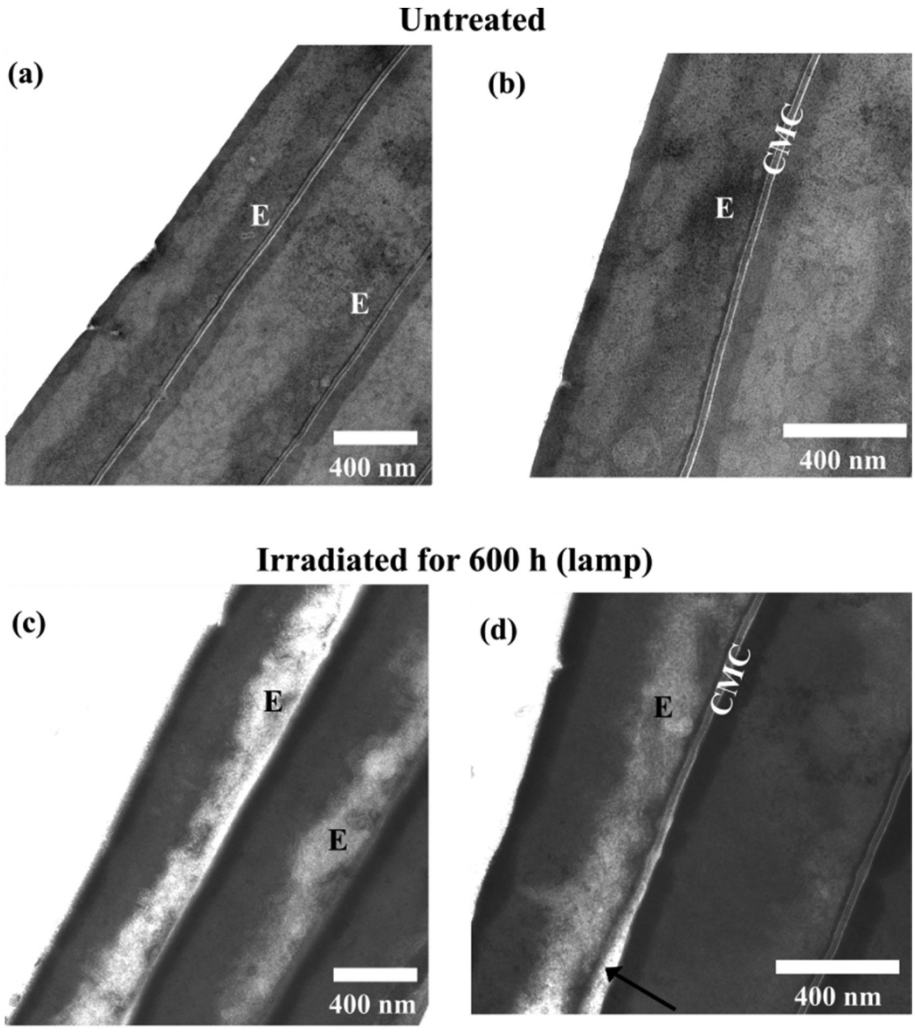

Fig. 7. Images of ultra-thin sections of the cuticle cells in blended white hair obtained by TEM: (a) and (b) untreated hair; (c) and (d) hair irradiated for 600 h with a mercury lamp. The rupture of the cell membrane complex (CMC) after irradiation is indicated in (d) and photo-damaged endocuticle (E) in (c).

This result indicates that amorphous regions were probably damaged by the irradiation, while microfibrils and protofibrils were not altered.

The main observation concerning the evolution of the ring scattering around 4.5 nm due to irradiation is that in samples that already presented this ring before irradiation, the ring became more intense after irradiation, as can be observed in Fig. 5 (e) and (f). This

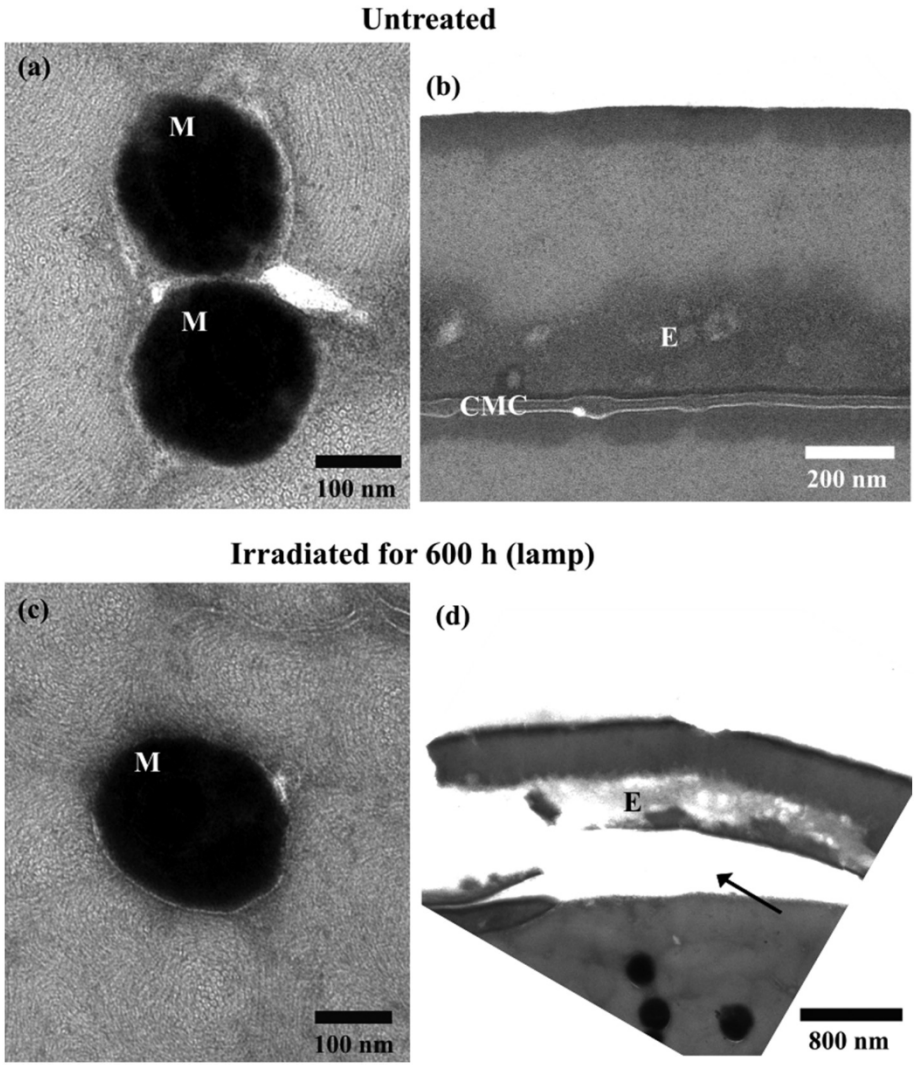

Fig. 8. Images of ultra-thin sections of the blended dark-brown hair obtained by TEM: (a) and (b) untreated hair; (c) and (d) hair irradiated for 600 h with a mercury lamp. Images show undifferentiated morphology of the melanin (M) after photo-radiation, damages in the endocuticle (E) and the rupture of cell membrane complex (CMC) indicated by the arrow in (d). There is resin from sample preparation between the cortex and the cuticle in (d), showing that the detachment of the cuticle was not caused by the sectioning procedure. (For interpretation of the references to colour in this figure legend, the reader is referred to the web version of this article.)

result showed that irradiation has an effect of organising the structures responsible for the ring scattering around 4.5 nm. However, it is important to highlight that the ring signal is not created by irradiation, it is just intensified in the samples where it was already present.

Also, SAXS patterns were measured in hair exposed to 75 h of solar radiation (Fig. S1 in supplementary material). Fig. S2(a-c) shows equatorial intensity profiles and Fig. S2(d-f) shows azimuthal intensity profiles from SAXS patterns of untreated and irradiated hair in Fig. S1. As occurred after lamp exposure, the diffuse scattering signal around 9 nm decreased (Fig. S2(a-c)) and the ring scattering around 4.5 nm increased after irradiation (arrows in Fig. S2).

Thus, the SAXS results can be summarised as follows: 1. there was a decrease in the intensity of the diffuse scattering after irradiation, which indicates photo-degradation of hair amorphous regions; 2. the intensity of the ring scattering around 4.5 nm increased after irradiation, but only in samples where the ring was already present before irradiation; 3. this scattering could not be attributed to the presence of free lipids, though the scattering due to covalently-bound lipids cannot be excluded; and 4. the positions of the two peaks at 9.3 nm and 4.8 nm in the equatorial profile were not altered after irradiation, showing that microfibrils and protofibrils did not undergo sufficient irradiation damage to lose their organisation.

3.2.2. Transmission Electron Microscopy (TEM)

Amorphous regions present in the cortex matrix and in the cuticle were investigated separately by TEM before and after irradiation. TEM images of ultrathin sections of white from blended hair (Fig. 7) and dark-brown from blended hair (Fig. 8) clearly showed a preferential degradation of the most external cuticle layer after 600 h of irradiation (Figs. 7 and 8(c) and (d)) in comparison to the untreated strands (Figs. 7 and 8(a) and (b)). Before irradiation, the endocuticle layers were continuous (darker areas indicated by E in Fig. 7(a) and (b) and in Fig. 8(b)), while after 600 h of irradiation, the outermost cuticle cell presented the most degraded (brighter) endocuticle when compared to the inner cuticle cells, as can be observed in Fig. 7(c) and (d) and in Fig. 8(d). CMC degradation as a consequence of irradiation was also observed, as indicated by the arrows in Figs. 7(d) and 8(d).

In previous work [3], we observed similar results concerning the degradation in the cuticle outermost layers and in CMC, using a different type of hair: dark-brown hair from a single donor. Our previous field emission scanning electron microscopy and TEM images showed that endocuticle and the CMC are the cuticle structures most degraded by irradiation and photo-degradation, as noticed by the occurrence of fracturing, cavities (Ø ≈ 20–200 nm) and cuticle cell lifting.

The general structure of the CMC is a central δ-layer covered on

both lateral sides by the lipid layers (inner and outer β-layers). The outer β-layer (located between δ-layer and epicuticle) contains 18-methyl eicosanoic acid (18-MEA) covalently bound to keratin by thioester linkages [11,13]. As indicated in Figs. 7(d) and 8(d), the outer β-layer begins to separate after 600 h of irradiation, which may be correlated to the ring scattering around 4.5 nm (SAXS results in Fig. 6(d – f)), since this is the region of covalently bound lipids.

On the other hand, TEM results did not show alterations in the cortex region, indicating that structural disintegration due to irradiation occurs mainly in the cuticle cells. Fig. 8(a) and (c) show images of melanin granules inside the cortex region of the blended dark-brown hair. Both before and after 600 h of irradiation, the melanin granules (indicated by M) were entire and unaltered. Thus, our experiments showed that photo-degradation was not enough to disrupt the cortex structures.

4. Conclusions

The results presented herewith showed that irradiation is especially harmful to the hair cuticle in both pigmented and non-pigmented hair, while the cortex shows no apparent structural degradation. Within the cuticle, the most affected parts are the endocuticle and the CMC, where rupture and other degradation signs are observed. SAXS showed the presence of a scattering ring around 4.5 nm in some hair samples, which increased in intensity after irradiation. Combined with TEM examination, these results suggest that this ring may be related to lipids present in the CMC and covalently bound to keratin by thioester linkages, but further experiments will be necessary to investigate this point.

Acknowledgements

The authors thank CAPES for financial support, also LNLS for the technical support during the small angle X-ray analysis.

Appendix A. Supplementary data

Supplementary data to this article can be found online at https://doi.org/10.1016/j.jphotobiol.2019.111673.

References

[1] S.B. Ruetsch, Y. Kamath, H.D. Weigmann, Photodegradation of human hair: a microscopy study, Comprehensive Series in Photosciences, Sun Protection in Man, 3 Elsevier science, London, 2001, pp. 175–205.
[2] M. Richena, C.A. Rezende, Effect of photodamage on the outermost cuticle layer of human hair, J. Photochem. Photobiol. B Biol. 153 (2015) 296–304.
[3] M. Richena, C.A. Rezende, Morphological degradation of human hair cuticle due to simulated sunlight irradiation and washing, J. Photochem Photobiol 161 (2016) 430–440.
[4] E. Hoting, M. Zimmermann, S. Hilterhaus-Bong, Photochemical alterations on human hair. Part I: artificial irradiation and investigations of hair proteins, J. Soc. Cosmet. Chem. 46 (1995) 85–99.
[5] E. Hoting, M. Zimmermann, H. Hocker, Photochemical alterations on human hair. Part II: analysis of melanin, J. Soc. Cosmet. Chem. 46 (1995) 181–190.
[6] E. Hoting, M. Zimmermann, Photochemical alterations in human hair. Part III. Investigations of internal lipids, J. Soc. Cosmet. Chem. 47 (1996) 201–211.
[7] J.E. Plowman, D.P. Harland, Fibre ultrastructure, in: J.E. Plowman, D.P. Harland, S. Deb-Choudhury (Eds.), The Hair Fibre: Proteins, Structure and Development, 1 Springer Nature, Singapore, 2018, pp. 3–13.
[8] G.E. Rogers, Electron Microscope Studies of Hair and Wool, vol. 83, Annals of the New York Academy of Sciences, 1959, pp. 378–399.
[9] J.A. Swift, A.W. Holmes, Degradation of human hair by papain part III. Some electron microscope observations, Text. Res. J. 35 (1965) 1014–1019.
[10] C.R. Robbins, Chemical and Physical Behavior of Human Hair, Springer-Verlag, New York, 2012.
[11] C.R. Robbins, The cell membrane complex: three related but different cellular cohesion components of mammalian hair fibers, J. Cosmet. Sci. 60 (2009) 437–465.
[12] J. Lindberg, B. Philip, N. Gralén, Occurrence of thin membranes in the structure of wool, Nature 162 (1948) 458–459.
[13] L.N. Jones, D.E. Rivett, The role of 18-methyleicosanoic acid in the structure and formation of mammalian hair fibres, Micron 28 (1997) 469–485.
[14] J.R. Smith, J.A. Swift, Lamellar subcomponents of the cuticular cell membrane complex of mammalian keratin fibres show friction and hardness contrast by AFM, J. Microsc. 206 (2002) 182–193.
[15] V. James, The molecular architecture for the intermediate filaments of hard α-keratin based on the superlattice data obtained from a study of mammals using synchrotron fibre diffraction, Biochem. Res. Int. 2011 (2011) 1–10.
[16] W.T. Astbury, A. Street, X-ray studies of the structure of hair, wool, and related fibres. I, General. Philoso. Trans. A 230 (1932) 75–101.
[17] L. Pauling, R.B. Corey, H.R. Branson, The structure of proteins: two hydrogen-bonded helical configurations of the polypeptide chain, Proc. Natl. Acad. Sci. 37 (1951) 261–271.
[18] P.M. Steinert, L.N. Marekov, R.D.B. Fraser, D.A.D. Parry, Keratin intermediate filament structure crosslinking studies yield quantitative information on molecular dimensions and mechanism of assembly, J. Mol. Biol. 230 (1993) 436–452.
[19] C.R. Robbins, M.J. Bahl, Analysis of hair by electron spectroscopy for chemical analysis, J. Soc. Cosmet. Chem. 35 (1984) 379–390.
[20] L.J. Wolfram, L. Albrecht, Chemical- and photo-bleaching of brown and red hair, J. Soc. Cosmet. Chem. 82 (1987) 179–191.
[21] C.M. Pande, J. Jachowicz, Hair photodamage – measurement and prevention, J. Soc. Cosmet. Chem. 44 (1993) 109–122.
[22] T. Gao, A. Bedell, Ultraviolet damage on natural gray hair and its photoprotection, J. Cosmet. Sci. 52 (2001) 103–118.
[23] A.C.S. Nogueira, I. Joekes, Hair color changes and protein damage caused by ultraviolet radiation, J. Photochem. Photobiol. B Biol. 74 (2004) 109–117.
[24] A.C.S. Nogueira, L. Dicelio, I. Joekes, About photo-damage of human hair, Photochem. Photobiol. Sci. 5 (2006) 165–169.
[25] A.C.S. Nogueira, M. Richena, L.E. Dicelio, I. Joekes, Photo yellowing of human hair, J. Photochem. Photobiol. B Biol. 88 (2007) 119–125.
[26] E. Fernández, C. Barba, C. Alonso, M. Martí, J.L. Parra, L. Coderch, Photodamage determination of human hair, J. Photochem. Photobiol. B Biol. 106 (2012) 101–106.
[27] J.H. Ji, T.S. Park, H.J. Lee, Y.D. Kim, L.Q. Pi, X.H. Jin, W.S. Lee, The ethnic differences of the damage of hair and integral lipid after ultra violet radiation, Ann. Dermatol. 25 (2013) 54–60.
[28] M. Richena, M. Silveira, C.A. Rezende, I. Joekes, Yellowing and bleaching of grey hair caused by photo and thermal degradation, J. Photochem. Photobiol. B Biol. 138 (2014) 172–181.
[29] T.C. Huang, H. Toraya, T.N. Blanton, Y. Wu, X-ray powder diffraction analysis of silver behenate, a possible low-angle diffraction standard, J. Appl. Crystallogr. 26 (1993) 180–184.
[30] R.D.B. Fraser, T.P. MacRae, G.E. Rogers, B.K. Filshie, Lipids in keratinized tissues, J. Mol. Biol. 7 (1963) 90–91.
[31] K.E. Wilk, V.J. James, Y. Amemiya, The intermediate filament structure of human hair, Biochim. Biophys. Acta 1245 (1995) 296–392.
[32] V. James, J. Kearsley, T. Irving, Y. Amemiya, D. Cookson, Using hair to screen for breast cancer, Nature 339 (1999) 33–34.
[33] P. Meyer, R. Goergl, J.W. Botz, P. Fratz, Breast Cancer screening using small-angle X-ray scattering analysis of human hair, JNCI 92 (2000) 1092–1093.
[34] F. Briki, B. Busson, B. Salicru, F. Esteve, J. Doucet, Breast-cancer diagnosis using hair, Nature 400 (1999) 226.
[35] B. Busson, P. Engstrom, J. Doucet, Existence of various structural zones in keratinous tissues revealed by X-ray microdiffraction, J. Synchrotron Radiat. 6 (1999) 1021–1030.
[36] M. Wade, I. Tucker, P. Cunningham, R. Skinner, F. Bell, T. Lyons, K. Patten, L. Gonzalez, T. Wess, Investigating the origins of nanostructural variations in differential ethnic hair types using X-ray scattering techniques, Int. J. Cosmet. Sci. 35 (2013) 1–12.
[37] L. Cordech, S. Mendez, C. Barba, R. Pons, M. Marti, J.L. Parra, Lamellar rearrangement of internal lipids from human hair, Chem. Phys. Lipids 155 (2008) 1–6.